

Measurement of Exclusive $\rho^+\rho^-$ Production in Mid-Virtuality Two-Photon Interactions and Study of the $\gamma\gamma^* \rightarrow \rho\rho$ Process at LEP

The L3 Collaboration

Abstract

Exclusive $\rho^+\rho^-$ production in two-photon collisions between a quasi-real photon, γ , and a mid-virtuality photon, γ^* , is studied with data collected at LEP at centre-of-mass energies $183 \text{ GeV} \leq \sqrt{s} \leq 209 \text{ GeV}$ with a total integrated luminosity of 684.8 pb^{-1} . The cross section of the $\gamma\gamma^* \rightarrow \rho^+\rho^-$ process is determined as a function of the photon virtuality, Q^2 , and the two-photon centre-of-mass energy, $W_{\gamma\gamma}$, in the kinematic region: $0.2 \text{ GeV}^2 \leq Q^2 \leq 0.85 \text{ GeV}^2$ and $1.1 \text{ GeV} \leq W_{\gamma\gamma} \leq 3 \text{ GeV}$. These results, together with previous L3 measurements of $\rho^0\rho^0$ and $\rho^+\rho^-$ production, allow a study of the $\gamma\gamma^* \rightarrow \rho\rho$ process over the Q^2 -region $0.2 \text{ GeV}^2 \leq Q^2 \leq 30 \text{ GeV}^2$.

Submitted to *Phys. Lett. B*

1 Introduction

The L3 Collaboration has recently measured the exclusive production of $\rho^0\rho^0$ [1,2] and $\rho^+\rho^-$ [3] pairs in the two-photon fusion process:

$$e^+e^- \rightarrow e^+e^-\gamma\gamma^* \rightarrow e^+e^-\rho\rho, \quad (1)$$

where the beam electrons¹⁾ radiate virtual photons which interact and produce a hadronic final state. One of the photons, γ , is quasi-real, characterised by a small value of its squared four momentum, $P_\gamma^2 = m_\gamma^2 \approx 0$, whereas the other one, γ^* , has a significant virtuality, $Q^2 = -P_{\gamma^*}^2 = -m_{\gamma^*}^2 \gg -m_\gamma^2$. Our measurements cover the two-photon centre-of-mass energy

$$1.1 \text{ GeV} \leq W_{\gamma\gamma} \leq 3 \text{ GeV}. \quad (2)$$

The two measurements [1,3] done at large virtualities, $1.2 \text{ GeV}^2 \leq Q^2 \leq 30 \text{ GeV}^2$, provide a testing ground for a recently-developed QCD-based model [4]. This model describes well the Q^2 -dependence of the $\rho^0\rho^0$ production at large momentum transfer [5]. The measured cross sections for $\rho^0\rho^0$ and $\rho^+\rho^-$ production were found to have a similar dependence on $W_{\gamma\gamma}$ and to be of similar magnitude. However, the $\rho^+\rho^-$ cross section is systematically higher than the $\rho^0\rho^0$ one. This is in contrast with the suppression and different $W_{\gamma\gamma}$ dependence of $\rho^+\rho^-$ production [6] with respect to $\rho^0\rho^0$ [7] observed in data with $Q^2 \approx 0$ and $W_{\gamma\gamma} \leq 2 \text{ GeV}$. We note that despite the wide range of theoretical models [8,9], ρ -pair production at $Q^2 \approx 0$ is still not well understood. Therefore the experimental study of the Q^2 -evolution of ρ -pair production is important to understand vector meson pair-production in two-photon interactions.

Previously, we performed a measurement of $\rho^0\rho^0$ production [2] for intermediate virtualities:

$$0.2 \text{ GeV}^2 \leq Q^2 \leq 0.85 \text{ GeV}^2. \quad (3)$$

In this Letter, we complement that study with the first measurement of the process:

$$e^+e^- \rightarrow e^+e^-\gamma\gamma^* \rightarrow e^+e^-\rho^+\rho^- \quad (4)$$

in the kinematic region (2) and (3). These data allow to follow the Q^2 -evolution of the $\rho\rho$ -production over two orders of magnitude in this variable.

The analysis techniques employed in this study are similar to those of our previous measurements [2,3]. The data used, corresponding to an integrated luminosity of 684.8 pb^{-1} , are the same as in Reference 2 and were collected by the L3 detector [10] at LEP at centre-of-mass energies $183 \text{ GeV} \leq \sqrt{s} \leq 209 \text{ GeV}$. Scattered beam electrons which have radiated photons with virtualities in the range (3) can be “tagged” by the Very Small Angle Tagger (VSAT) [11]. The VSAT is an electromagnetic calorimeter, constructed with BGO crystals, with a geometrical acceptance covering the polar angle range $5 \text{ mrad} \leq \theta \leq 10 \text{ mrad}$, for azimuthal angles in the ranges $-1.25 \text{ rad} \leq \phi \leq 1.25 \text{ rad}$ and $\pi - 1.25 \text{ rad} \leq \phi \leq \pi + 1.25 \text{ rad}$. When the electron with the largest scattering angle is detected in the VSAT, the virtuality of the photon it radiated is, within 1% precision, equal to the transverse momentum squared, p_t^2 , of the final state hadron system:

$$Q^2 = 2E_b E_s (1 - \cos \theta_s) \approx E_b E_s \theta_s^2 \approx p_t^2, \quad (5)$$

where E_b is the beam energy, and E_s and θ_s are the energy and the scattering angle of the tagged electron. Therefore the VSAT is not used to directly measure Q^2 , but rather to select exclusive final states by correlating the direction of the transverse momentum vector of the tagged electron with the detected hadron system.

¹⁾Throughout this Letter, the term “electron” denotes both electron and positron.

2 Event Selection

The reaction $e^+e^- \rightarrow e^+e^-\rho^+\rho^-$ contributing to the process

$$e^+e^- \rightarrow e^+e_{\text{tag}}^-\pi^+\pi^-\pi^0\pi^0 \quad (6)$$

is identified by one and only one scattered electron, e_{tag} , detected in the VSAT, two charged pions measured in the tracking chamber, and energy clusters from the two-photon decays of the π^0 's, deposited in the BGO electromagnetic calorimeter. These events are collected by two independent track-triggers [12]. The trigger efficiency, as determined from the data itself, is $(60 \pm 3)\%$.

Single-tagged events are selected by requiring just one electromagnetic cluster with energy greater than 50% of the beam energy reconstructed in the VSAT. The event candidates must have exactly two tracks with zero total charge. The tracks must come from the interaction vertex, have transverse momentum greater than 100 MeV and an energy loss in the tracking chamber compatible with the pion hypothesis. The selected events should contain a $\pi^0\pi^0$ pair, therefore we consider event candidates that have four or five photons, identified as isolated clusters in the electromagnetic calorimeter. Photons having energies greater than 60 MeV are paired to reconstruct neutral pions, which are required to be in the mass window $100 \text{ MeV} \leq M(\gamma\gamma) \leq 170 \text{ MeV}$, as shown in Figure 1a. The mass of a π^0 candidate is constrained to the nominal value by a 1-C kinematic fit. If more than one $\pi^0\pi^0$ combination exists, the one with the smallest χ^2 sum of the fits is taken. To make the selection robust against instrumental noise and backgrounds and to reduce the sensitivity to the Monte Carlo simulation of fake photons, we retain events with one additional photon, not used in the $\pi^0\pi^0$ pair, if the photon energy is less than 300 MeV and does not exceed 10% of the energy of the $\pi^0\pi^0$ pair.

The transverse momentum squared, p_t^2 , of the four-pion system is used to measure the Q^2 of the event and is required to be in the range $0.2 \text{ GeV}^2 - 0.85 \text{ GeV}^2$. For selection of an exclusive final state, the acoplanarity angle, ϕ_{aco} , calculated from the difference between the azimuthal angle of the tagged electron, ϕ_{tag} , shown in Figure 1b, and the azimuthal angle of the four-pion system, is required to be less than 0.4 rad, as shown in Figure 1c. The data contain a contribution from η production, as visible in the $\pi^+\pi^-\pi^0$ mass spectrum, shown in Figure 1d. This background is removed by requiring $M(\pi^+\pi^-\pi^0) > 0.65 \text{ GeV}$.

After all cuts, 414 events are retained. Their four-pion mass spectrum is shown in Figure 2a. The region $1.1 \text{ GeV} \leq W_{\gamma\gamma} \leq 3 \text{ GeV}$ is populated by 387 events, which are used for the cross section determination. A strong signal from ρ^\pm production is observed in the $M(\pi^\pm\pi^0)$ spectrum, shown in Figure 2b. The clustering of entries at the crossing of the ρ^\pm mass bands in the correlation plot of the masses of the $\pi^\pm\pi^0$ combinations, shown in Figure 2c, gives evidence for a signal from $\rho^+\rho^-$ intermediate states. No structure is observed in the correlation plot of the masses of the $\pi^+\pi^-$ and $\pi^0\pi^0$ combinations, shown in Figure 2d. We also inspected the two- and three-pion mass distributions, shown in Figure 3, for production of higher-mass resonances. The only statistically-significant signal is from the $a_2^\pm(1320)$ state in the $\pi^\pm\pi^0\pi^0$ mass spectrum, as seen in Figure 3f.

3 Data Analysis

3.1 Monte Carlo Modelling

To estimate the number of $\rho^+\rho^-$ events in the selected four-pion data sample, we consider non-interfering contributions from the processes:

$$\begin{aligned}
 \gamma\gamma^* &\rightarrow \rho^+\rho^-; \\
 \gamma\gamma^* &\rightarrow \rho^\pm\pi^\mp\pi^0; \\
 \gamma\gamma^* &\rightarrow a_2^\pm(1320)\pi^\mp; \\
 \gamma\gamma^* &\rightarrow \pi^+\pi^-\pi^0\pi^0, \text{ non-resonant.}
 \end{aligned}
 \tag{7}$$

About 40 million Monte Carlo events of the processes (7) are generated with the EGPC [13] program, which uses the luminosity function from Reference 14. Particle production and decay is uniform in phase-space. The generated events are passed through the full L3 detector simulation using the GEANT [15] and GHEISHA [16] programs and processed in the same way as the data, reproducing the detector behaviour as monitored in the different data-taking periods.

For acceptance calculations, Monte Carlo events are assigned a Q^2 -dependent weight, evaluated using the GVDM form-factor [17] for both interacting photons. The detection efficiencies of the process (4) are listed in Tables 1 and 2 for bins in Q^2 and $W_{\gamma\gamma}$. The efficiencies for the four-pion final states of all the processes (7) are of similar magnitude.

3.2 Background Estimation

The contribution to the selected events from e^+e^- annihilation and from the process $e^+e^- \rightarrow e^+e^-\tau^+\tau^-$ is negligible. Random coincidences with off-momentum beam electrons, which give signals in the VSAT, are a source of background. The flux of these particles is dominantly on the outer side of the LEP ring. Therefore, this background would cause an excess in the number of events having a tag on the outer side of the accelerator ring, N_{out} , with respect to the inner side, N_{in} . In the selected data, the ratio $N_{out}/N_{in} = 1.04 \pm 0.10$ is close to unity, indicating that this background is small. This conclusion is corroborated by the good agreement observed between the ϕ_{tag} distribution of the selected data and Monte Carlo event samples, shown in Figure 1b.

Two sources of background remain. The first is partially-reconstructed events from two-photon interactions with higher particle multiplicities, when tracks or photons escape detection. The second is signal events with one or more photons substituted by photon candidates due to noise. To estimate the accepted background we use background-like event samples extracted from the experimental data. The first background is modelled with selected $\pi^\pm\pi^\pm\pi^0\pi^0$ events, in which at least two charged particles have not been detected and by $\pi^+\pi^-\pi^0\pi^0$ events in which one π^0 is excluded from consideration. An event-mixing technique is employed in order to reproduce events from the second background: one or two photons forming a π^0 are excluded from a selected event and replaced by photons from another data event. The ϕ_{aco} distributions of the background-like data samples, passing the selection, are combined with the distribution of selected $\pi^+\pi^-\pi^0\pi^0$ Monte Carlo events so as to reproduce the ϕ_{aco} distribution observed in the data, as shown in Figures 1c. The estimated background levels are listed in Tables 1 and 2. As data samples are used in the background estimation, they contain also a fraction of events with fake tags and thus take into account the effect of this background.

3.3 Fit Method

In order to determine the differential $\rho^+\rho^-$ production rate, a maximum likelihood fit of the data to a sum of Monte Carlo samples of the processes (7) is performed in intervals of Q^2 and $W_{\gamma\gamma}$ using a box method [1–3, 18]. The inputs to the fit are the six two-pion masses in an event, namely the four combinations $\pi^\pm\pi^0$ and the two combinations $\pi^+\pi^-$ and $\pi^0\pi^0$. They provide a complete description of a four-pion event in our model of isotropic production and phase space decay.

The analysis procedure is optimised for deriving the $\rho^+\rho^-$ contribution and only the $\rho^+\rho^-$ content and the sum of the rest of the contributing processes, denoted as “other 4π ”, are considered for cross section measurements. To check the quality of the fit, the two- and three-pion mass distributions of the data are compared in Figure 3 with those of a mixture of Monte Carlo event samples from the processes (7), in proportions determined by the fit. The observed experimental distributions are reasonably well described by the Monte Carlo model.

4 Results

The cross sections of the process $e^+e^- \rightarrow e^+e^-\rho^+\rho^-$ in bins of Q^2 and $W_{\gamma\gamma}$, $\Delta\sigma_{ee}$, are listed in Tables 1 and 2. The statistical uncertainties, also listed in Tables 1 and 2, are those of the fit. The differential cross section, $d\sigma_{ee}/dQ^2$, derived from $\Delta\sigma_{ee}$, is listed in Table 1. When evaluating the differential cross section, a correction based on the Q^2 -dependence of the $\rho^+\rho^-$ Monte Carlo sample is applied, so as to assign the cross section value to the centre of the corresponding Q^2 -bin [19].

To evaluate the cross section, $\sigma_{\gamma\gamma}$, of the process $\gamma\gamma^* \rightarrow \rho^+\rho^-$, the integral of the transverse photon luminosity function, L_{TT} , is computed for each Q^2 and $W_{\gamma\gamma}$ bin using the program GALUGA [20], which performs $\mathcal{O}(\alpha^4)$ QED calculations. The same procedure was used in our previous studies [1–3]. The cross section $\sigma_{\gamma\gamma}$ is derived from the measured cross section using the relation $\sigma_{\gamma\gamma} = \Delta\sigma_{ee}/L_{TT}$. Thus, $\sigma_{\gamma\gamma}$ represents an effective cross section containing contributions from both transverse and longitudinal photon polarisations. The cross section of the process $\gamma\gamma^* \rightarrow \rho^+\rho^-$ is listed in Table 1 as a function of Q^2 and in Table 2 as a function of $W_{\gamma\gamma}$. The sum of the cross sections of the other contributing processes is also given in Tables 1 and 2.

Several sources of systematic uncertainty are considered. The contribution of the selection procedure is in the range 12% – 18%; Monte Carlo statistics in the range 1.3% – 2.1%; the fit procedure in the range 11% – 20%. Half of the changes of the acceptance when no form factor re-weighting of the Monte Carlo events is performed is considered as model uncertainty. It is in the range 0.5% – 5%. The background correction procedure introduces systematic uncertainties in the range 2% – 6%. All contributions are added in quadrature to obtain the systematic uncertainties, quoted in Tables 1 and 2. Finally, a normalization uncertainty of 5% accounts for the uncertainty of the trigger efficiency determination.

5 Study of $\gamma\gamma^* \rightarrow \rho\rho$ Process

Combining the present results with the L3 data on $\rho\rho$ production from References 1–3, we compare the $\rho^+\rho^-$ to the $\rho^0\rho^0$ channels and their evolution as a function of Q^2 . The cross section of the process $\gamma\gamma^* \rightarrow \rho\rho$ is plotted in Figure 4 as a function of $W_{\gamma\gamma}$. For $W_{\gamma\gamma} \leq 2.1$ GeV and $0.2 \text{ GeV}^2 \leq Q^2 \leq 0.85 \text{ GeV}^2$ there is a clear enhancement of $\rho^0\rho^0$ production

relative to $\rho^+\rho^-$. This is similar to what was observed at $Q^2 \approx 0$ [6, 7], but in contrast with the high Q^2 -region, where both cross sections have similar dependence on $W_{\gamma\gamma}$ and the $\rho^+\rho^-$ is systematically higher than the $\rho^0\rho^0$. These differences are clearly seen in the ratio $R = \sum \Delta\sigma_{ee}(\rho^+\rho^-) / \sum \Delta\sigma_{ee}(\rho^0\rho^0)$ where the sum is for the region $1.1 \text{ GeV} \leq W_{\gamma\gamma} \leq 2.1 \text{ GeV}$. In the domain $0.20 \text{ GeV}^2 \leq Q^2 \leq 0.85 \text{ GeV}^2$, we measure $R = 0.62 \pm 0.10$ (stat.) ± 0.09 (syst.), a value that can only be explained by the presence of an isospin $I = 2$ intermediate state or by a mixture of different states [8, 9]. The value of this ratio for $1.2 \text{ GeV}^2 \leq Q^2 \leq 8.5 \text{ GeV}^2$ is $R = 1.81 \pm 0.47$ (stat.) ± 0.22 (syst.) [3], close to the factor 2, expected for an isospin $I = 0$ state. Such variation suggests different ρ -pair production mechanisms at low and high Q^2 .

The differential cross section $d\sigma_{ee}/dQ^2$ of the reaction $e^+e^- \rightarrow e^+e^-\rho\rho$ is shown in Figure 5a. The L3 measurements span a Q^2 -region of two orders of magnitude, over which the differential cross sections show a monotonic fall of more than four orders of magnitude. The $\rho\rho$ data are fitted to a form [21] expected from QCD-based calculations [22]:

$$\frac{d\sigma_{ee}}{dQ^2} \sim \frac{1}{Q^n(Q^2 + \langle W_{\gamma\gamma} \rangle)^2}, \quad (8)$$

where n is a constant and $\langle W_{\gamma\gamma} \rangle$ is the average $W_{\gamma\gamma}$ value, 1.9 GeV for this measurement. Although this formula is expected to be valid only for $Q^2 \gg W_{\gamma\gamma}$, we find it provides a good parametrisation of the Q^2 -evolution of the $\rho\rho$ data. A fit to the $\rho^+\rho^-$ data finds an exponent $n = 2.3 \pm 0.2$ with $\chi^2/d.o.f. = 1.4/7$. A value $n = 2.9 \pm 0.1$ was found for $\rho^0\rho^0$ with $\chi^2/d.o.f. = 6.9/10$ [2]. Only the statistical uncertainties are considered in the fits. The results of the fits are shown in Figure 5a. The fits indicate a cross-over of the differential cross sections of $\rho^+\rho^-$ and $\rho^0\rho^0$ production in the vicinity of $Q^2 \approx 1 \text{ GeV}^2$.

The measured cross section of the process $\gamma\gamma^* \rightarrow \rho\rho$ as a function of Q^2 is shown in Figure 5b. The change of the relative magnitude of $\rho^+\rho^-$ and $\rho^0\rho^0$ production is clearly visible when comparing the low- and the high- Q^2 regions. A parametrisation, based on the GVDM model [17]:

$$\sigma_{\gamma\gamma}(W_{\gamma\gamma}, Q^2) = \sigma_{\gamma\gamma}(W_{\gamma\gamma})F(Q^2), \quad \text{and} \quad F(Q^2) = \sum_{V=\rho,\omega,\phi} r_V \frac{1 + Q^2/4m_V^2}{(1 + Q^2/m_V^2)^2} + \frac{0.22}{1 + Q^2/m_0^2}, \quad (9)$$

with $r_\rho = 0.65, r_\omega = 0.08, r_\phi = 0.05$ and $m_0 = 1.4 \text{ GeV}$ reproduces well the Q^2 -dependence of the $\rho^0\rho^0$ data, as shown in Reference 2 and indicated by the line in Figure 5b. The fit finds a cross section of $13.6 \pm 0.7 \text{ nb}$ for the $W_{\gamma\gamma}$ region $1.1 \text{ GeV} \leq W_{\gamma\gamma} \leq 3 \text{ GeV}$ at $Q^2 = 0$. The Q^2 -evolution of $\rho^+\rho^-$ data cannot be satisfactorily described by this form. In addition, as shown in Figure 5b, the $\rho^0\rho^0$ data cannot be described by the much steeper Q^2 -fall of a ρ -pole parametrisation [2]; the same is true for the $\rho^+\rho^-$ cross section since it is decreasing with Q^2 less steeply than the $\rho^0\rho^0$ one.

6 Conclusions

We have performed the first measurement of exclusive $\rho^+\rho^-$ production in mid-virtuality two-photon collisions. These results complement previous L3 measurements of exclusive $\rho^+\rho^-$ and $\rho^0\rho^0$ production and allow to follow the evolution of $\rho\rho$ cross sections over a Q^2 -region of two orders of magnitude.

A QCD-based form, derived for the description of the differential cross-section $d\sigma_{ee}/dQ^2$ of the process $e^+e^- \rightarrow e^+e^-\rho\rho$ at high Q^2 , is found to provide a good parametrisation of the

Q^2 -evolution of the $\rho\rho$ data in the entire interval $0.2 \text{ GeV}^2 \leq Q^2 \leq 30 \text{ GeV}^2$, over which the differential cross sections show a monotonic decrease of more than four orders of magnitude, for $1.1 \text{ GeV} \leq W_{\gamma\gamma} \leq 3 \text{ GeV}$.

The Q^2 -dependence of the cross section of the process $\gamma\gamma^* \rightarrow \rho^0\rho^0$ is well reproduced by a parametrisation based on the GVDM model over the entire Q^2 -region. On the other hand, the $\rho^+\rho^-$ data cannot be satisfactorily described by such a parametrisation. A ρ -pole description of the Q^2 -dependence for both $\rho^0\rho^0$ and $\rho^+\rho^-$ data is excluded.

The relative magnitude of $\rho^+\rho^-$ and $\rho^0\rho^0$ production changes in the vicinity of $Q^2 \approx 1 \text{ GeV}^2$, suggesting different ρ -pair production mechanisms at low and high Q^2 .

References

- [1] L3 Coll., P. Achard *et al.*, Phys. Lett. B **568** (2003) 11.
- [2] L3 Coll., P. Achard *et al.*, Phys. Lett. B **604** (2004) 48.
- [3] L3 Coll., P. Achard *et al.*, Phys. Lett. B **597** (2004) 26.
- [4] M. Diehl *et al.*, Phys. Rev. Lett. **81** (1998) 1782; N. Kivel, L. Mankiewicz and M.V. Polyakov, Phys. Lett. B **467** (1999) 263; A. Freund, Phys. Rev. D **61** (2000) 074010.
- [5] I.V. Anikin, B. Pire and O.V. Teryaev, Phys. Rev. D **69** (2004) 014018.
- [6] ARGUS Coll., H. Albrecht *et al.*, Phys. Lett. B **217** (1989) 205; Phys. Lett. B **267** (1991) 535; CELLO Coll., H.-J. Behrend *et al.*, Phys. Lett. B **218** (1989) 493.
- [7] TASSO Coll., R. Brandelik *et al.*, Phys. Lett. B **97** (1980) 448; M. Althoff *et al.*, Z. Phys. C **16** (1982) 13; MARK II Coll., D.L. Burke *et al.*, Phys. Lett. B **103** (1981) 153; CELLO Coll., H.-J. Behrend *et al.*, Z. Phys. C **21** (1984) 205; TPC/Two-Gamma Coll., H. Aihara *et al.*, Phys. Rev. D **37** (1988) 28; PLUTO Coll., Ch. Berger *et al.*, Z. Phys. C **38** (1988) 521; ARGUS Coll., H. Albrecht *et al.*, Z. Phys. C **50** (1991) 1.
- [8] N.N. Achasov *et al.*, Phys. Lett. B **108** (1982) 134; Z. Phys. C **16** (1982) 55; Phys. Lett. B **203** (1988) 309; G. Alexander *et al.*, Phys. Rev. D **26** (1982) 1198; Z. Phys. C **30** (1986) 65; B.A. Li and K.F. Liu, Phys. Lett. B **118** (1982) 435; Phys. Lett. B **124** (1983) 550; Phys. Rev. D **30** (1984) 613; Phys. Rev. Lett. **58** (1987) 2288; S.J. Brodsky, G. Köpp and P.M. Zerwas, Phys. Rev. Lett. **58** (1987) 443.
- [9] J.L. Rosner Phys. Rev. D **70** (2004) 034028.
- [10] L3 Coll., B. Adeva *et al.*, Nucl. Instr. Meth. A **289** (1990) 35; M. Chemarin *et al.*, Nucl. Instr. Meth. A **349** (1994) 345; M. Acciarri *et al.*, Nucl. Instr. Meth. A **351** (1994) 300; I.C. Brock *et al.*, Nucl. Instr. Meth. A **381** (1996) 236; A. Adam *et al.*, Nucl. Instr. Meth. A **383** (1996) 342.
- [11] T. van Rhee, Ph.D. thesis, University of Utrecht (1999).
- [12] P. Béné *et al.*, Nucl. Instr. Meth. A **306** (1991) 150; D. Haas *et al.*, Nucl. Instr. Meth. A **420** (1999) 101.
- [13] F.L. Linde, Ph.D. thesis, Rijksuniversiteit Leiden (1988).

- [14] V.M. Budnev *et al.*, Phys. Rep. C **15** (1975) 181.
- [15] GEANT version 3.21 is used; R. Brun *et al.*, CERN report CERN DD/EE/84-1 (1984), revised 1987.
- [16] GHEISHA, H. Fesefeldt, RWTH Aachen report PITHA 85/2 (1985).
- [17] J.J. Sakurai and D. Schildknecht, Phys. Lett. B **40** (1972) 121; I.F. Ginzburg and V.G. Serbo, Phys. Lett. B **109** (1982) 231.
- [18] D.M. Schmidt, R.J. Morrison and M.S. Witherell, Nucl. Instr. Meth. A **328** (1993) 547.
- [19] G.D. Lafferty and T.R. Wyatt, Nucl. Instr. Meth. A **355** (1995) 541.
- [20] G.A. Schuler, Comput. Phys. Commun. **108** (1998) 279.
- [21] M. Diehl, private communication.
- [22] M. Diehl, T. Gousset and B. Pire, Phys. Rev. D **62** (2000) 073014.

The L3 Collaboration:

P.Achard,²⁰ O.Adriani,¹⁷ M.Aguilar-Benitez,²⁵ J.Alcaraz,²⁵ G.Alemanni,²³ J.Allaby,¹⁸ A.Aloisio,²⁹ M.G.Alvigi,²⁹ H.Anderhub,⁴⁹ V.P.Andreev,^{6,34} F.Anselmo,⁸ A.Arefiev,²⁸ T.Azemoon,³ T.Aziz,⁹ P.Bagnaia,³⁹ A.Bajo,²⁵ G.Baksay,²⁶ L.Baksay,²⁶ S.V.Baldew,² S.Banerjee,⁹ Sw.Banerjee,⁴ A.Barczyk,^{49,47} R.Barillère,¹⁸ P.Bartolini,²³ M.Basile,⁸ N.Batalova,⁴⁶ R.Battiston,³³ A.Bay,²³ F.Becattini,¹⁷ U.Becker,¹³ F.Behner,⁴⁹ L.Bellucci,¹⁷ R.Berbeco,³ J.Berdugo,²⁵ P.Berges,¹³ B.Bertucci,³³ B.L.Betev,⁴⁹ M.Biasini,³³ M.Biglietti,²⁹ A.Biland,⁴⁹ J.J.Blaising,⁴ S.C.Blyth,³⁵ G.J.Bobbink,² A.Böhm,¹ L.Boldizar,¹² B.Borgia,³⁹ S.Bottai,¹⁷ D.Bourilkov,⁴⁹ M.Bourquin,²⁰ S.Braccini,²⁰ J.G.Branson,⁴¹ F.Brochu,⁴ J.D.Burger,¹³ W.J.Burger,³³ X.D.Cai,¹³ M.Capell,¹³ G.Cara Romeo,⁸ G.Carlino,²⁹ A.Cartacci,¹⁷ J.Casaus,²⁵ F.Cavallari,³⁹ N.Cavallo,³⁶ C.Cecchi,³³ M.Cerrada,²⁵ M.Chamizo,²⁰ Y.H.Chang,⁴⁴ M.Chemarin,²⁴ A.Chen,⁴⁴ G.Chen,⁷ G.M.Chen,⁷ H.F.Chen,²² H.S.Chen,⁷ G.Chiefari,²⁹ L.Cifarelli,⁴⁰ F.Cindolo,⁸ I.Clare,¹³ R.Clare,³⁸ G.Coignet,⁴ N.Colino,²⁵ S.Costantini,³⁹ B.de la Cruz,²⁵ S.Cucciarelli,³³ R.de Asmundis,²⁹ P.Déglon,²⁰ J.Debreczeni,¹² A.Degré,⁴ K.Dehmelt,²⁶ K.Deiters,⁴⁷ D.della Volpe,²⁹ E.Delmeire,²⁰ P.Denes,³⁷ F.DeNotaristefani,³⁹ A.De Salvo,⁴⁹ M.Diemoz,³⁹ M.Dierckxsens,² C.Dionisi,³⁹ M.Dittmar,⁴⁹ A.Doria,²⁹ M.T.Dova,^{10,‡} D.Duchesneau,⁴ M.Duda,¹ B.Echenard,²⁰ A.Eline,¹⁸ A.El Hage,¹ H.El Mamouni,²⁴ A.Engler,³⁵ F.J.Eppling,¹³ P.Extermann,²⁰ M.A.Falagan,²⁵ S.Falciano,³⁹ A.Favara,³² J.Fay,²⁴ O.Fedin,³⁴ M.Felcini,⁴⁹ T.Ferguson,³⁵ H.Fesefeldt,¹ E.Fiandrini,³³ J.H.Field,²⁰ F.Filthaut,³¹ P.H.Fisher,¹³ W.Fisher,³⁷ I.Fisk,⁴¹ G.Forconi,¹³ K.Freundreich,⁴⁹ C.Furetta,²⁷ Yu.Galaktionov,^{28,13} S.N.Ganguli,⁹ P.Garcia-Abia,²⁵ M.Gataullin,³² S.Gentile,³⁹ S.Giagu,³⁹ Z.F.Gong,²² G.Grenier,²⁴ O.Grimm,⁴⁹ M.W.Gruenewald,¹⁶ M.Guida,⁴⁰ V.K.Gupta,³⁷ A.Gurtu,⁹ L.J.Gutay,⁴⁶ D.Haas,⁵ D.Hatzifotiadou,⁸ T.Hebbeker,¹ A.Hervé,¹⁸ J.Hirschfelder,³⁵ H.Hofer,⁴⁹ M.Hohlmann,²⁶ G.Holzner,⁴⁹ S.R.Hou,⁴⁴ B.N.Jin,⁷ P.Jindal,¹⁴ L.W.Jones,³ P.de Jong,² I.Josa-Mutuberría,²⁵ M.Kaur,¹⁴ M.N.Kienzle-Focacci,²⁰ J.K.Kim,⁴³ J.Kirkby,¹⁸ W.Kittel,³¹ A.Klimentov,^{13,28} A.C.König,³¹ M.Kopal,⁴⁶ V.Koutsenko,^{13,28} M.Kräber,⁴⁹ R.W.Kraemer,³⁵ A.Krüger,⁴⁸ A.Kunin,¹³ P.Ladron de Guevara,²⁵ I.Laktineh,²⁴ G.Landi,¹⁷ M.Lebeau,¹⁸ A.Lebedev,¹³ P.Lebrun,²⁴ P.Lecomte,⁴⁹ P.Lecoq,¹⁸ P.Le Coultre,⁴⁹ J.M.Le Goff,¹⁸ R.Leiste,⁴⁸ M.Levtchenko,²⁷ P.Levtchenko,³⁴ C.Li,²² S.Likhoded,⁴⁸ C.H.Lin,⁴⁴ W.T.Lin,⁴⁴ F.L.Linde,² L.Lista,²⁹ Z.A.Liu,⁷ W.Lohmann,⁴⁸ E.Longo,³⁹ Y.S.Lu,⁷ C.Luci,³⁹ L.Luminari,³⁹ W.Lustermann,⁴⁹ W.G.Ma,²² L.Malgeri,¹⁸ A.Malinin,²⁸ C.Maña,²⁵ J.Mans,³⁷ J.P.Martin,²⁴ F.Marzano,³⁹ K.Mazumdar,⁹ R.R.McNeil,⁶ S.Mele,^{18,29} L.Merola,²⁹ M.Meschini,¹⁷ W.J.Metzger,³¹ A.Mihul,¹¹ H.Milcent,¹⁸ G.Mirabelli,³⁹ J.Mnich,¹ G.B.Mohanty,⁹ G.S.Muanza,²⁴ A.J.M.Muijs,² B.Musicar,⁴¹ M.Musy,³⁹ S.Nagy,¹⁵ S.Natale,²⁰ M.Napolitano,²⁹ F.Nessi-Tedaldi,⁴⁹ H.Newman,³² A.Nisati,³⁹ T.Novak,³¹ H.Nowak,⁴⁸ R.Ofierzynski,⁴⁹ G.Organtini,³⁹ I.Pal,⁴⁶ C.Palomares,²⁵ P.Paolucci,²⁹ R.Paramatti,³⁹ G.Passaleva,¹⁷ S.Patricelli,²⁹ T.Paul,¹⁰ M.Pauluzzi,³³ C.Paus,¹³ F.Pauss,⁴⁹ M.Pedace,³⁹ S.Pensotti,²⁷ D.Perret-Gallix,⁴ D.Piccolo,²⁹ F.Pierella,⁸ M.Pioppi,³³ P.A.Piroué,³⁷ E.Pistoiesi,²⁷ V.Plyaskin,²⁸ M.Pohl,²⁰ V.Pojidaev,¹⁷ J.Pothier,¹⁸ D.Prokofiev,³⁴ G.Rahal-Callot,⁴⁹ M.A.Rahaman,⁹ P.Raics,¹⁵ N.Raja,⁹ R.Ramelli,⁴⁹ P.G.Rancoita,²⁷ R.Ranieri,¹⁷ A.Raspereza,⁴⁸ P.Razis,³⁰ D.Ren,⁴⁹ M.Rescigno,³⁹ S.Reucroft,¹⁰ S.Riemann,⁴⁸ K.Riles,³ B.P.Roe,³ L.Romero,²⁵ A.Rosca,⁴⁸ C.Rosemann,¹ C.Rosenbleck,¹ S.Rosier-Lees,⁴ S.Roth,¹ J.A.Rubio,¹⁸ G.Ruggiero,¹⁷ H.Ryckaczewski,⁴⁹ A.Sakharov,⁴⁹ S.Saremi,⁶ S.Sarkar,³⁹ J.Salicio,¹⁸ E.Sanchez,²⁵ C.Schäfer,¹⁸ V.Schegelsky,³⁴ H.Schopper,²¹ D.J.Schotanus,³¹ C.Sciacca,²⁹ L.Servoli,³³ S.Shevchenko,³² N.Shivarov,⁴² V.Shoutko,¹³ E.Shumilov,²⁸ A.Shvorob,³² D.Son,⁴³ C.Souga,²⁴ P.Spillantini,¹⁷ M.Steuer,¹³ D.P.Stickland,³⁷ B.Stoyanov,⁴² A.Straessner,²⁰ K.Sudhakar,⁹ G.Sultanov,⁴² L.Z.Sun,²² S.Sushkov,¹ H.Suter,⁴⁹ J.D.Swain,¹⁰ Z.Szillasi,^{26,¶} X.W.Tang,⁷ P.Tarjan,¹⁵ L.Tauscher,⁵ L.Taylor,¹⁰ B.Tellili,²⁴ D.Teyssier,²⁴ C.Timmermans,³¹ Samuel C.C.Ting,¹³ S.M.Ting,¹³ S.C.Tonwar,⁹ J.Tóth,¹² C.Tully,³⁷ K.L.Tung,⁷ J.Ulbricht,⁴⁹ E.Valente,³⁹ R.T.Van de Walle,³¹ R.Vasquez,⁴⁶ V.Veszpremi,²⁶ G.Vesztergombi,¹² I.Vetlitsky,²⁸ G.Viertel,⁴⁹ S.Villa,³⁸ M.Vivargent,⁴ S.Vlachos,⁵ I.Vodopianov,²⁶ H.Vogel,³⁵ H.Vogt,⁴⁸ I.Vorobiev,^{35,28} A.A.Vorobyov,³⁴ M.Wadhwa,⁵ Q.Wang,³¹ X.L.Wang,²² Z.M.Wang,²² M.Weber,¹⁸ S.Wynhoff,³⁷ L.Xia,³² Z.Z.Xu,²² J.Yamamoto,³ B.Z.Yang,²² C.G.Yang,⁷ H.J.Yang,³ M.Yang,⁷ S.C.Yeh,⁴⁵ An.Zalite,³⁴ Yu.Zalite,³⁴ Z.P.Zhang,²² J.Zhao,²² G.Y.Zhu,⁷ R.Y.Zhu,³² H.L.Zhuang,⁷ A.Zichichi,^{8,18,19} B.Zimmermann,⁴⁹ M.Zöller,¹

- 1 III. Physikalisches Institut, RWTH, D-52056 Aachen, Germany[§]
 - 2 National Institute for High Energy Physics, NIKHEF, and University of Amsterdam, NL-1009 DB Amsterdam, The Netherlands
 - 3 University of Michigan, Ann Arbor, MI 48109, USA
 - 4 Laboratoire d'Annecy-le-Vieux de Physique des Particules, LAPP,IN2P3-CNRS, BP 110, F-74941 Annecy-le-Vieux CEDEX, France
 - 5 Institute of Physics, University of Basel, CH-4056 Basel, Switzerland
 - 6 Louisiana State University, Baton Rouge, LA 70803, USA
 - 7 Institute of High Energy Physics, IHEP, 100039 Beijing, China[△]
 - 8 University of Bologna and INFN-Sezione di Bologna, I-40126 Bologna, Italy
 - 9 Tata Institute of Fundamental Research, Mumbai (Bombay) 400 005, India
 - 10 Northeastern University, Boston, MA 02115, USA
 - 11 Institute of Atomic Physics and University of Bucharest, R-76900 Bucharest, Romania
 - 12 Central Research Institute for Physics of the Hungarian Academy of Sciences, H-1525 Budapest 114, Hungary[‡]
 - 13 Massachusetts Institute of Technology, Cambridge, MA 02139, USA
 - 14 Panjab University, Chandigarh 160 014, India
 - 15 KLTE-ATOMKI, H-4010 Debrecen, Hungary[¶]
 - 16 Department of Experimental Physics, University College Dublin, Belfield, Dublin 4, Ireland
 - 17 INFN Sezione di Firenze and University of Florence, I-50125 Florence, Italy
 - 18 European Laboratory for Particle Physics, CERN, CH-1211 Geneva 23, Switzerland
 - 19 World Laboratory, FBLJA Project, CH-1211 Geneva 23, Switzerland
 - 20 University of Geneva, CH-1211 Geneva 4, Switzerland
 - 21 University of Hamburg, D-22761 Hamburg, Germany
 - 22 Chinese University of Science and Technology, USTC, Hefei, Anhui 230 029, China[△]
 - 23 University of Lausanne, CH-1015 Lausanne, Switzerland
 - 24 Institut de Physique Nucléaire de Lyon, IN2P3-CNRS, Université Claude Bernard, F-69622 Villeurbanne, France
 - 25 Centro de Investigaciones Energéticas, Medioambientales y Tecnológicas, CIEMAT, E-28040 Madrid, Spain^b
 - 26 Florida Institute of Technology, Melbourne, FL 32901, USA
 - 27 INFN-Sezione di Milano, I-20133 Milan, Italy
 - 28 Institute of Theoretical and Experimental Physics, ITEP, Moscow, Russia
 - 29 INFN-Sezione di Napoli and University of Naples, I-80125 Naples, Italy
 - 30 Department of Physics, University of Cyprus, Nicosia, Cyprus
 - 31 Radboud University and NIKHEF, NL-6525 ED Nijmegen, The Netherlands
 - 32 California Institute of Technology, Pasadena, CA 91125, USA
 - 33 INFN-Sezione di Perugia and Università Degli Studi di Perugia, I-06100 Perugia, Italy
 - 34 Nuclear Physics Institute, St. Petersburg, Russia
 - 35 Carnegie Mellon University, Pittsburgh, PA 15213, USA
 - 36 INFN-Sezione di Napoli and University of Potenza, I-85100 Potenza, Italy
 - 37 Princeton University, Princeton, NJ 08544, USA
 - 38 University of California, Riverside, CA 92521, USA
 - 39 INFN-Sezione di Roma and University of Rome, "La Sapienza", I-00185 Rome, Italy
 - 40 University and INFN, Salerno, I-84100 Salerno, Italy
 - 41 University of California, San Diego, CA 92093, USA
 - 42 Bulgarian Academy of Sciences, Central Lab. of Mechatronics and Instrumentation, BU-1113 Sofia, Bulgaria
 - 43 The Center for High Energy Physics, Kyungpook National University, 702-701 Taegu, Republic of Korea
 - 44 National Central University, Chung-Li, Taiwan, China
 - 45 Department of Physics, National Tsing Hua University, Taiwan, China
 - 46 Purdue University, West Lafayette, IN 47907, USA
 - 47 Paul Scherrer Institut, PSI, CH-5232 Villigen, Switzerland
 - 48 DESY, D-15738 Zeuthen, Germany
 - 49 Eidgenössische Technische Hochschule, ETH Zürich, CH-8093 Zürich, Switzerland
- § Supported by the German Bundesministerium für Bildung, Wissenschaft, Forschung und Technologie.
‡ Supported by the Hungarian OTKA fund under contract numbers T019181, F023259 and T037350.
¶ Also supported by the Hungarian OTKA fund under contract number T026178.
^b Supported also by the Comisión Interministerial de Ciencia y Tecnología.
[‡] Also supported by CONICET and Universidad Nacional de La Plata, CC 67, 1900 La Plata, Argentina.
[△] Supported by the National Natural Science Foundation of China.

Q^2 range [GeV ²]	ε [%]	Bg [%]	$\Delta\sigma_{ee}$ [pb] $\rho^+\rho^-$	$d\sigma_{ee}/dQ^2$ [pb/GeV ²] $\rho^+\rho^-$	$\sigma_{\gamma\gamma}$ [nb] $\rho^+\rho^-$	$\sigma_{\gamma\gamma}$ [nb] other 4π
0.20 – 0.28	0.8	14	$7.4 \pm 2.4 \pm 1.9$	$92 \pm 29 \pm 23$	$5.7 \pm 1.8 \pm 1.4$	$10.9 \pm 2.2 \pm 1.5$
0.28 – 0.40	1.2	14	$5.7 \pm 1.8 \pm 1.3$	$47 \pm 15 \pm 10$	$4.3 \pm 1.4 \pm 1.0$	$12.2 \pm 1.8 \pm 1.4$
0.40 – 0.55	1.1	15	$5.6 \pm 1.6 \pm 1.1$	$37 \pm 11 \pm 7.3$	$4.9 \pm 1.4 \pm 1.0$	$13.3 \pm 2.0 \pm 1.8$
0.55 – 0.85	0.7	18	$7.7 \pm 2.5 \pm 2.0$	$25 \pm 8.2 \pm 6.5$	$5.3 \pm 1.7 \pm 1.4$	$12.1 \pm 2.2 \pm 1.9$

Table 1: Detection efficiencies, ε , background fractions, Bg , and cross sections of the reactions $e^+e^- \rightarrow e^+e^-\rho^+\rho^-$, $\gamma\gamma^* \rightarrow \rho^+\rho^-$ and of the sum of the rest of the contributing processes, "other 4π ", as a function of Q^2 for $1.1 \text{ GeV} \leq W_{\gamma\gamma} \leq 3 \text{ GeV}$. The values of the differential cross sections are corrected to the centre of each bin. The first uncertainties are statistical, the second systematic. An overall normalization uncertainty of 5% for the trigger is not included.

$W_{\gamma\gamma}$ -range [GeV]	ε [%]	Bg [%]	$\Delta\sigma_{ee}$ [pb] $\rho^+\rho^-$	$\sigma_{\gamma\gamma}$ [nb] $\rho^+\rho^-$	$\sigma_{\gamma\gamma}$ [nb] other 4π
1.10 – 1.40	0.6	25	$4.9 \pm 1.8 \pm 1.3$	$3.9 \pm 1.5 \pm 1.1$	$9.0 \pm 2.4 \pm 1.7$
1.40 – 1.65	0.9	18	$6.7 \pm 1.6 \pm 1.3$	$7.6 \pm 1.9 \pm 1.5$	$14.8 \pm 2.7 \pm 2.5$
1.65 – 1.85	1.1	15	$5.1 \pm 1.5 \pm 0.9$	$8.4 \pm 2.4 \pm 1.6$	$15.8 \pm 3.1 \pm 2.3$
1.85 – 2.10	1.1	13	$3.9 \pm 1.4 \pm 0.8$	$5.9 \pm 2.0 \pm 1.2$	$18.3 \pm 3.0 \pm 2.7$
2.10 – 2.40	1.2	10	$2.2 \pm 1.0 \pm 0.5$	$3.2 \pm 1.4 \pm 0.8$	$11.5 \pm 2.1 \pm 1.8$
2.40 – 3.00	1.2	10	$2.2 \pm 1.0 \pm 0.5$	$1.9 \pm 0.9 \pm 0.5$	$8.5 \pm 1.5 \pm 1.5$

Table 2: Detection efficiencies, ε , background fractions, Bg , and cross sections of the reactions $e^+e^- \rightarrow e^+e^-\rho^+\rho^-$, $\gamma\gamma^* \rightarrow \rho^+\rho^-$ and of the sum of the rest of the contributing processes, other 4π , as a function of $W_{\gamma\gamma}$ for $0.2 \text{ GeV}^2 \leq Q^2 \leq 0.85 \text{ GeV}^2$. The first uncertainties are statistical, the second systematic. An overall normalization uncertainty of 5% for the trigger is not included.

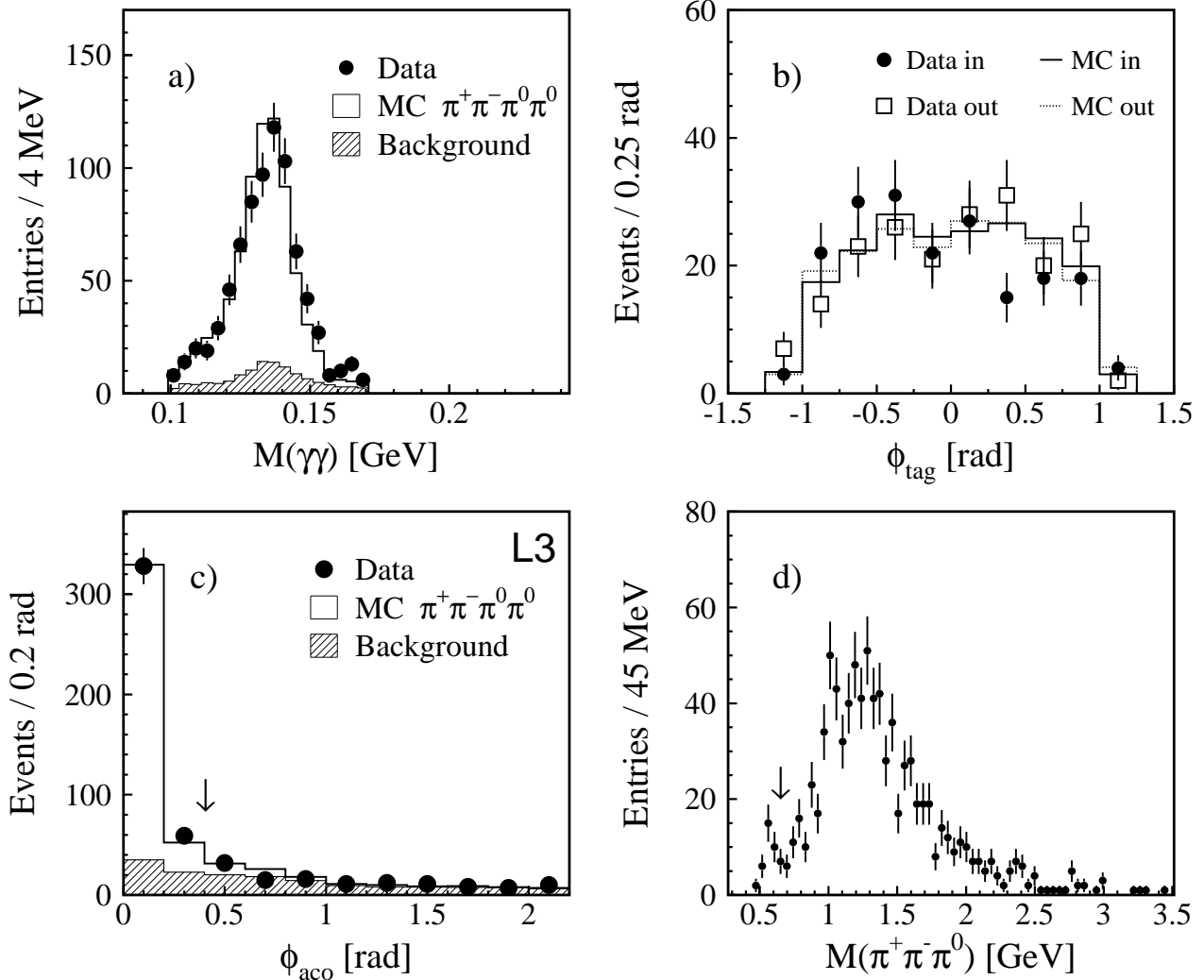


Figure 1: Distributions for $\pi^+\pi^-\pi^0\pi^0$ candidates. a) Two-photon invariant mass for the selected π^0 's (two entries per event); b) azimuthal angle, ϕ_{tag} , of the tagged electron for tags in the inner side of the LEP ring (in) and, folded over it, for tags in the outer side of the LEP ring (out); c) acoplanarity angle, ϕ_{aco} , between the tagged electron and the $\pi^+\pi^-\pi^0\pi^0$ system and d) mass of the $\pi^+\pi^-\pi^0$ system (two entries per event). The data are compared to the four-pion Monte Carlo. The estimated background is indicated by the hatched histograms. The arrows indicate the selection cuts.

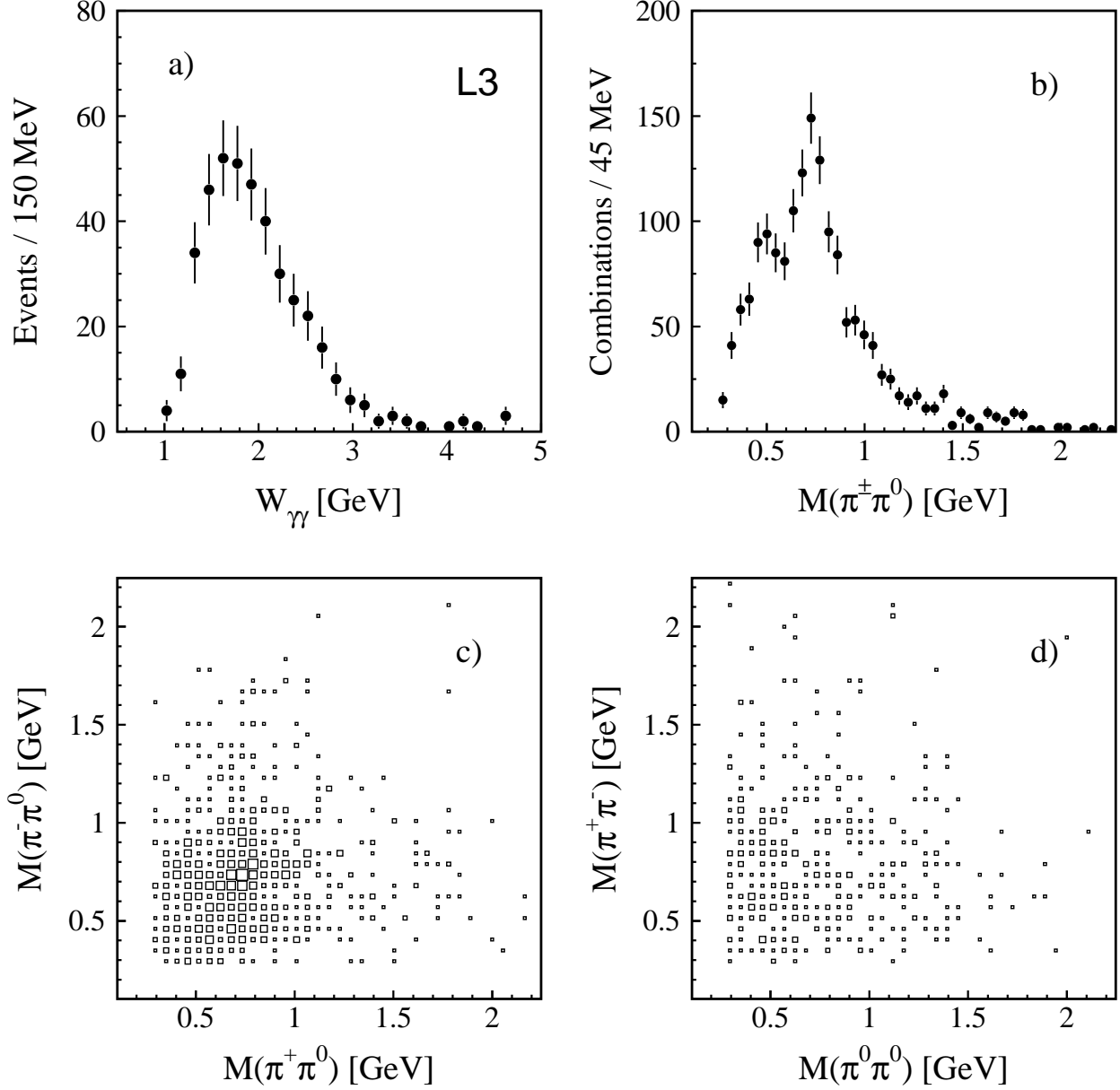


Figure 2: Mass distributions for the selected events: a) the four-pion system, W_{γ} ; b) the $\pi^{\pm}\pi^0$ combinations (four entries per event); c) correlation between the $\pi^-\pi^0$ and $\pi^+\pi^0$ pairs (two entries per event) and d) correlation between the $\pi^+\pi^-$ and $\pi^0\pi^0$ pairs. The two-dimensional distributions have a bin width of $55 \times 55 \text{ MeV}^2$, the size of the boxes is proportional to the number of entries and both plots have the same vertical scale.

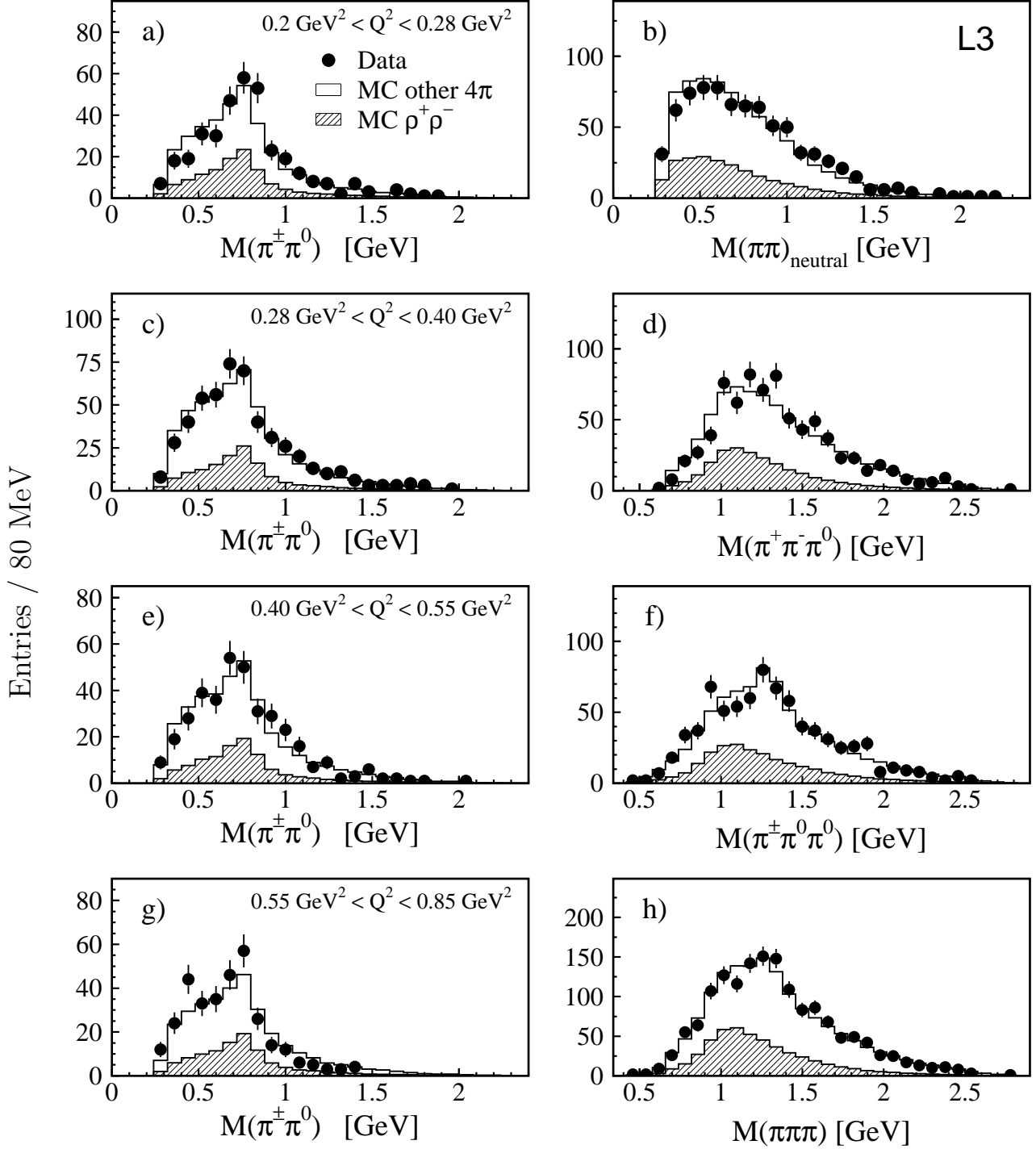


Figure 3: a),c),e),g) Mass distributions of the $\pi^\pm\pi^0$ combinations (four entries per event) in four Q^2 -intervals and distributions for the entire kinematic region $1.1 \text{ GeV} \leq W_{\gamma\gamma} \leq 3 \text{ GeV}$ and $0.2 \text{ GeV}^2 \leq Q^2 \leq 0.85 \text{ GeV}^2$ of b) The sum of the $\pi^+\pi^-$ and $\pi^0\pi^0$ mass spectra (two entries per event). d) The neutral three-pion combinations (two entries per event). f) The charged three-pion combinations (two entries per event). h) The sum of the $\pi^+\pi^-\pi^0$ and $\pi^\pm\pi^0\pi^0$ mass spectra (four entries per event). The points represent the data, the hatched areas show the $\rho^+\rho^-$ component and the open areas show the sum of the other contributing processes. The fraction of the different components are determined by the fit and the total normalisation is to the number of the events.

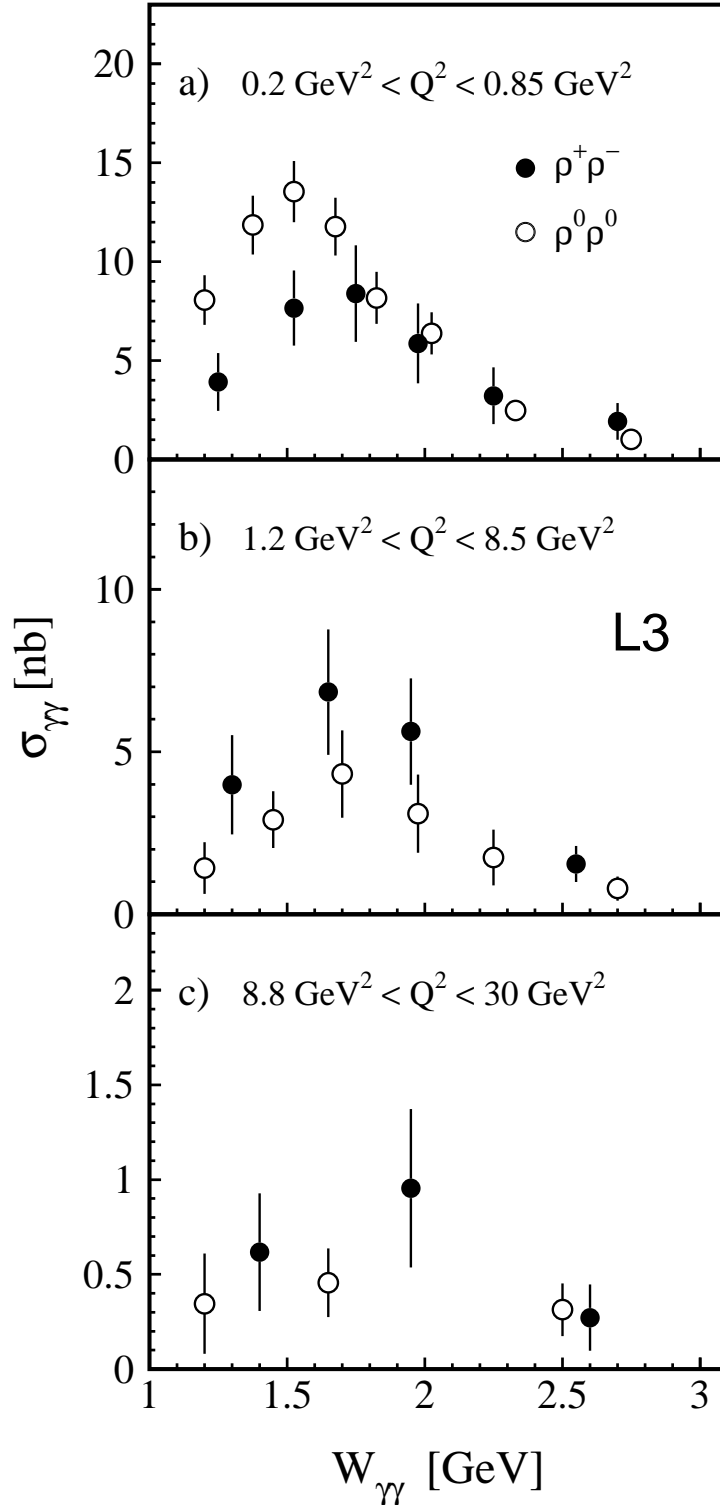


Figure 4: Cross section of the process $\gamma\gamma^* \rightarrow \rho\rho$ as a function of $W_{\gamma\gamma}$ in three Q^2 regions. The results from this measurement, full points in a), are compared to previous L3 measurements of the $\rho\rho$ production [1–3]. The bars show the statistical uncertainties. Some points from the previous measurements are displaced horizontally for better readability.

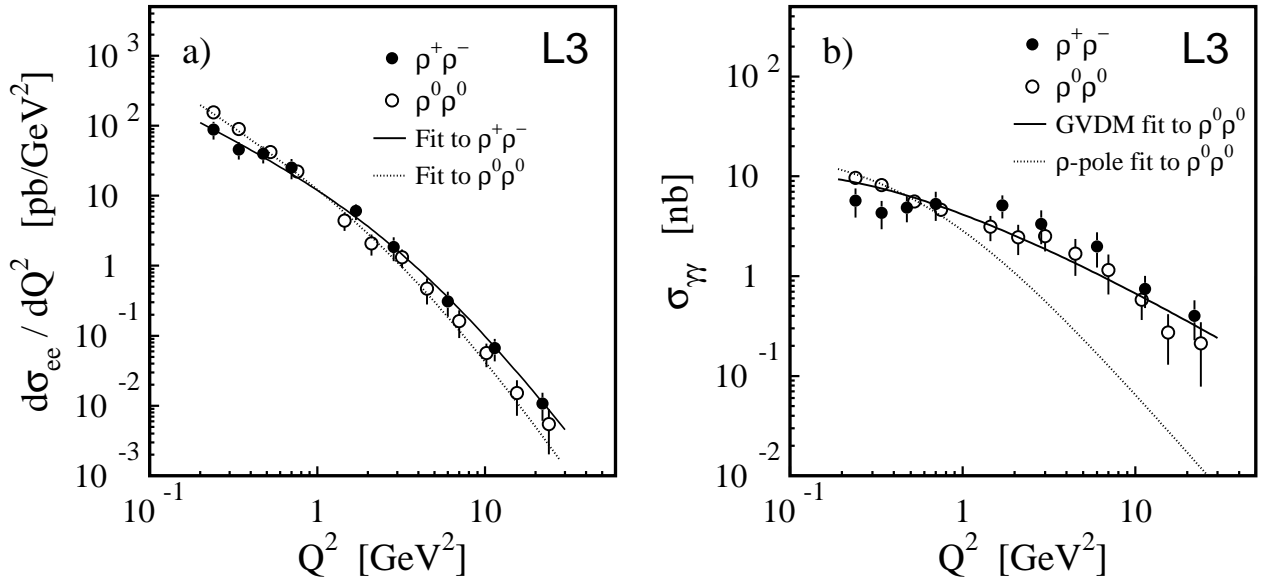


Figure 5: The $\rho\rho$ production cross section as a function of Q^2 , for $1.1 \text{ GeV} \leq W_{\gamma\gamma} \leq 3 \text{ GeV}$: a) differential cross section of the process $e^+e^- \rightarrow e^+e^-\rho\rho$ and b) cross section of the process $\gamma\gamma^* \rightarrow \rho\rho$. The results from this measurement, full points in the region $Q^2 < 1 \text{ GeV}^2$, are presented together with previous L3 measurements of the $\rho\rho$ production [1–3]. The bars indicate the statistical uncertainties. Some points from the previous measurements are displaced horizontally for better readability. The lines in a) represent the results of fits using the QCD-inspired form of equation (9). The lines in b) represent the results of a fit to the $\rho^0\rho^0$ data based on the GVDM model [17] and of a fit based on a ρ -pole parametrisation.